Articles

Glutathione Induces Helical Formation in the Carboxy Terminus of Human Glutathione Transferase A1-1†

Yiping Zhan and Gordon S. Rule*

Department of Biological Sciences, Carnegie Mellon University, 4400 Fifth Avenue, Pittsburgh, Pennsylvania 15213

Received December 30, 2003; Revised Manuscript Received March 4, 2004

ABSTRACT: The structure and dynamic properties of the C-terminal region of the human class alpha glutathione transferase A1-1 have been investigated with high-resolution NMR methods. On the basis of crystallographic and fluorescence measurements, this 13-residue segment of the enzyme is presumed to be disordered in the unliganded enzyme. When the product or product analogue is bound, a C-terminal α-helix is observed in crystal structures. Conflicting data exists regarding the structure of this region when one of the substrates, glutathione (GSH), is bound. The NMR studies presented here show that in the unliganded protein, this region of the protein samples different conformations, most likely an ensemble of helix-like structures. Addition of either GSH or the conjugate between GSH and ethacrynic acid (EASG) causes this segment to become a stable α-helix. In the GSH complex, the ends of this helix exhibit dynamic behavior on both the millisecond and nanosecond time scales. In contrast, there is no evidence of millisecond dynamics in the EASG complex. The ligand-induced ordering of the enzyme reduces the intrinsic affinity of the enzyme for its product, facilitating enzymatic turnover.

Glutathione transferases (GSTs,[1] EC 2.5.1.18) constitute a large family of cytosolic and membrane-bound proteins that catalyze the conjugation of glutathione (GSH, γ-Glu-Cys-Gly) to a variety of endogenous and exogenous electrophiles. Typical reactions include the displacement of chlorine from 1-chloro-2,4-dinitrobenzene (CDNB) or the addition of GSH to activated double bonds, such as in ethacrynic acid (see Scheme 1). GSTs play an important role in detoxification by inactivating hydrophobic compounds that contain reactive centers. A single isoform is capable of conjugating GSH to a number of hydrophobic substrates. This plasticity in substrate specificity, when coupled with the large number of isozymes, generates an impressively large range of potential substrates. The cytosolic GSTs are grouped into eight gene classes based on sequence similarities and substrate specificities: alpha, kappa, mu, omega, pi, sigma, theta, and zeta (*1*−*7*). Each class contains one or more members. GSTs exist in the form of homodimers or intraclass heterodimers, with an overall molecular mass of approximately 50 kDa. The composition of each dimer is specified by stating the class and isoform, prefaced by the species identification. Thus, hGSTA1-1 is a homodimeric human enzyme composed of isoform 1 from the alpha class, and rGSTA1-1 is the homologous enzyme from rat.

Scheme 1

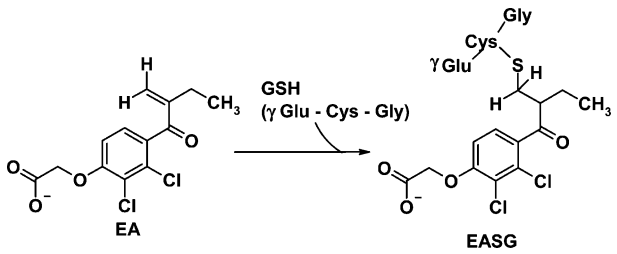

Overexpression of some isoforms of GST is involved in the development of drug resistance in tumor cells due to their catalytic ability towards chemotherapeutic drugs (*8*−*10*). The catalytic activity of a GST is also important for the biosynthesis of GSH conjugates, such as leukotriene A (*1*). GSTs are also known to have ligandin activity, or the ability to bind to a variety of hydrophobic compounds without catalytic turnover (*11*). This activity is considered important in the sequestering and transportation of nonpolar ligands. Recently, GSTs were reported to be involved in the regulation of cell division and apoptosis via binding to protein kinases in signal transduction pathways (*12*, *13*).

A number of X-ray crystal structures have been determined for GSTs (*7*, *15*−*25*). GSTs from different classes share a common global fold. Each subunit has two domains, an amino-terminal domain of 70−80 residues of mixed α-helical and β-strand structure and a carboxy-terminal domain of 120−140 residues that is predominantly α-helical. The N-terminal domain contains the GSH-binding site (G-site). The hydrophobic substrate-binding site (H-site) is formed by residues from both the C-terminal and N-terminal domains. The G-site is relatively conserved across different

† Supported by Grant GM61253 from the National Institutes of Health and the Eberly Chair in Structural Biology.

* To whom correspondence should be addressed. E-mail: rule@andrew.cmu.edu. Fax: (412) 268-7129. Telephone: (412) 268-1839.

[1] Abbreviations: GST, glutathione transferase; GSH, glutathione; GOH, γ-Glu-Ser-Gly; GS-Me, *S*-methylglutathione; CDNB, 1-chloro-2,4-dinitrobenzene; EA, ethacrynic acid; EASG, conjugate between GSH and EA; hGSTA1-1, homodimeric GST alpha from humans, isoform 1; rGSTA1-1, homodimeric hGSTA1-1 from rat.

10.1021/bi0363329 CCC: $27.50
Published on Web 05/21/2004

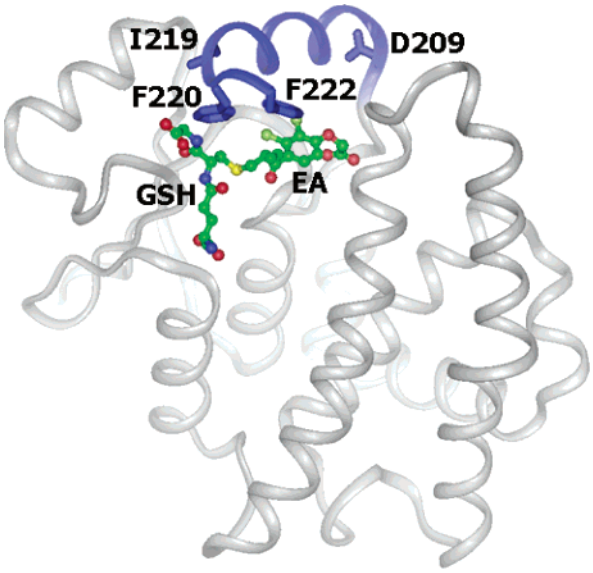

FIGURE 1: Diagram highlighting interactions of the C-terminal helix (blue) with EASG in a subunit of hGSTA1-1. The bound product, EASG, is labeled and shown in ball-and-stick format. EASG forms a van der Waals contact with the side chain of Phe222. The side chains of Asp209, Ile219, and Phe220 are also labeled. This diagram was generated from crystal structure 1GSE (*15*) using InsightII (Accelrys). Only one of the two conformations of EASG in the original crystal structure is shown.

Scheme 2

$$E + EASG \underset{k_{-1}}{\overset{k_1}{\rightleftharpoons}} \underset{\text{Disordered}}{[E\text{-}EASG]} \underset{k_{-2}}{\overset{k_2}{\rightleftharpoons}} \underset{\text{Ordered}}{[E\text{-}EASG]}$$

GST classes. However, the H-site shows considerable variation in both structure and sequence. A unique feature of the alpha class GST is an amphipathic α-helix at the C-terminus of the enzyme that forms part of the H-site.

For hGSTA1-1, crystal structures have shown that the C-terminal α-helix cannot be identified in the unliganded form of the protein because of weak electron density (*15*, *25*). This C-terminal helix is observed when the enzyme is complexed with *S*-benzylglutathione, ethacrynic acid (EA), the ethacrynic acid−glutathione conjugate (EASG), or *S*-hexylglutathione (*15*, *16*, *25*). The C-terminal helix has also been observed in an altered position in glutathione sulfonate-bound rGSTA1-1, where it appears to be stabilized by crystal packing (*26*). Figure 1 shows the binding of one diastereoisomer of EASG to hGSTA1-1 and highlights some of the interactions between the ligand and the C-terminal helix. To date, no structures have been reported for GSH-bound hGSTA1-1.

In addition to crystallographic studies, a number of different techniques have been used to investigate the properties of the C-terminus in hGSTA1-1. Using stopped-flow fluorescence experiments, Nieslanik et al. (*27*, *28*) established a two-step mechanism for binding of EASG to hGSTA1-1 for both human and rat enzymes. As illustrated in Scheme 2, there is an initial rapid ligand docking step followed by a second step that is attributed to isomerization of the carboxy-terminal helix from a disordered state to a more ordered state. This hypothesis is supported by the fact that removal of the C-terminal residues appears to eliminate the second kinetic step.

Scheme 3

$$E^* \overset{\text{FAST}}{\rightleftharpoons} E \underset{k_{-2}}{\overset{k_2}{\rightleftharpoons}} [E\text{-}GSH]$$

The involvement of individual residues in the kinetic mechanism has been addressed with mutagenesis experiments. Replacement of Phe220 with Tyr or Ile affects both kinetic steps with the largest change associated with the reverse reaction, k_{-2}. Conversion of Phe220 to Tyr decreased k_{-2} by a factor of 2.0, while replacement with Ile increased k_{-2} by a factor of 2.8 (*28*).

Thermodynamic parameters were also obtained from stopped-flow studies. In the case of the F222W/W21F rGSTA1-1 enzyme, the docking step is entropy-driven and presumably associated with desolvation, while the second step is enthalpy-driven and is presumed to involve localization of the C-terminal helix. The enthalpy associated with the second step was −13 kJ/mol for rGSTA1-1, suggesting the formation of a number of contacts between the ligand and the enzyme. The formation of the ordered E−EASG state is favored. However, at equilibrium, a significant fraction appears to exist in the disordered state, approximately 10% for both the human and rat forms.

Stopped-flow experiments have also been performed to study the kinetics of binding of GSH to hGSTA1-1 and several C-terminal mutants (*29*). In contrast to the situation with EASG, the data for GSH are best described by a fast equilibrium between multiple states of the enzyme, of which only a subset can bind GSH, as illustrated in Scheme 3. Note that this model does not exclude the possibility of an isomerization step that follows the binding of GSH; however it would have to be either rapid or spectroscopically silent. The on-rate of GSH binding was found to be much lower than the diffusion limit and was increased in mutants that were predicted to make the C-terminal helix less stable. On the basis of this work, the C-terminus of the unliganded enzyme is believed to undergo transitions between different conformations, restricting the access of GSH to the active site. Alteration of Phe220 to Ala increased the off-rate of GSH by a factor of 3.2, suggesting a direct involvement of Phe220 in GSH binding (*29*).

It is unclear at this time whether GSH, upon binding to hGSTA1-1, stabilizes the C-terminal helix. Fluorescence spectroscopy was used to probe binding of GSH to a W21F/F222W mutant of rGSTA1-1. It was found that EA, EASG, and *S*-hexylglutathione, all of which are known to stabilize the C-terminal helix, induce the expected changes in the fluorescence spectrum from the carboxyl-terminal Trp residue. In contrast, GSH and glutathione sulfonate did not have any effect on the fluorescence of this Trp residue. It was thus argued that even if the G-site is occupied by GSH, the C-terminus remains delocalized and possibly disordered (*26*). However, by using the anionic dye ANS to monitor the presence of hydrophobic surfaces of hGSTA1-1, Dirr et al. (*30*) found that GSH stabilizes the C-terminal conformation more than EA, although not as much as the conjugate product. Experiments performed in the presence of low denaturant (urea) concentrations show that enzyme activity can be used to monitor subtle conformational changes of the enzyme that occur prior to global unfolding. Available evidence suggests that the decrease in enzyme activity is due to loss of the helix structure at the C-terminus (*30*). Addition

of GSH or the product shifts the midpoint of the urea-induced transition in enzyme activity to higher concentrations, suggesting that both GSH and the product stabilize the C-terminus of the enzyme (*30*). Several studies (*30*−*32*) show that the C-terminus does not contribute in a significant fashion to the overall thermodynamic stability of the enzyme; however, structuring of the C-terminus appears to be the final step in the refolding of the enzyme. Finally, Allardyce et al. (*33*) also identified a GSH-induced conformational change in the H-site and showed that the C-terminal helix plays a role in this process.

The C-terminal region of both class alpha and mu enzymes may play an important role in defining the rate-limiting step for catalysis. Studies on rGSTA1-1 by Nieslanik et al. (*27*) showed that at low temperatures the rate of the reverse of the first binding step (k_{-1}) was equal to the turnover number for the enzyme. Armstrong and co-workers have characterized product release in the class mu enzyme from rat, rGSTM1-1. In this case, the turnover number with CDNB as a substrate was found to be equal to the off-rate of the product. The slow off-rate was attributed to a hydrogen bond between a Tyr and a C-terminal Thr residue, generating a structural cap over the bound product. Removal of the hydrogen bond by conversion of the Tyr to Phe increased both the turnover rate and the off-rate, presumably by disruption of the hydrogen bond (*34*). Recent hydrogen exchange studies have shown that the Tyr to Phe mutation showed an increased level of segmental motion in the region of the active site (*35*).

Elucidation of the structure and function of the unique C-terminal helix of class alpha GST remains an open problem. NMR, as a method for studying the solution structure and dynamics of proteins, offers information that cannot be obtained from high-resolution X-ray crystal structures or fluorescence studies. In particular, techniques are available for studying slow motions that are associated with chemical exchange, on the time scale of 0.1−10 ms as well as fast motion, on the time scale of picoseconds to nanoseconds.

Preliminary NMR studies on hGSTA1-1 were reported by Lian (*36*, *37*). In that study, the protein was labeled with [^{15}N]Phe and resonance lines from the 10 Phe residues in the protein were assigned by site-directed mutagenesis. The chemical shifts of the Phe amide groups were used to detect changes in the environment of the Phe residues due to binding of GSH, CDNB, and the conjugate formed between GSH and CDNB.

More extensive NMR studies of hGSTA1-1 face the challenges posed by the large size of the dimeric molecule (51 kDa). However, using a combination of sample labeling techniques, such as perdeuteration and specific labeling, and automated methods for NMR assignments (*38*), we have shown that it is possible to obtain reliable backbone assignments of a number of GST isoforms (*39*, *40*). In this report, we have used NMR to characterize the structure and dynamics of the C-terminal residues of hGSTA1-1 for the unliganded, GSH-bound, and EASG-bound forms. Our results show that the C-terminus of the unliganded enzyme undergoes chemical exchange and samples an ensemble of helix-like conformations. Surprisingly, in the GSH-bound form, the C-terminal helix is completely formed, except that it is more flexible at its ends than in the EASG-bound form.

We have also explored the relationship between the thermodynamics of local unfolding and the binding of the product. In the case of the human class pi enzyme, hGSTP1-1, it was previously shown that a substantial region of the active site becomes ordered when GSH is bound to the enzyme, decreasing the entropy of the enzyme (*40*). The favorable change in entropy that occurs upon product release provides a mechanism for reducing the overall affinity of the product, thus facilitating recycling of the enzyme.

Here, we show that the free energy of binding of EASG to hGSTA1-1 is substantial (−40 kJ/mol) and is approximately equal to the sum of the free energies of binding for both substrates. Consequently, the product is tightly bound to the enzyme, and the ligand-induced folding of the C-terminus of hGSTA1-1 provides a mechanism for lowering the affinity of the enzyme for its product in a manner similar to that of hGSTP1-1. However, in contrast to the situation with GSTP1-1, the temperature dependence of the ligand-induced folding is small, which is consistent with a smaller region of hGSTA1-1 undergoing a disorder-to-order transition.

MATERIALS AND METHODS

Sample Preparation. An efficient expression system for recombinant hGSTA1-1 was kindly supplied by B. Mannervik (*41*). The C112S mutant was generated from this plasmid using a site-directed mutagenesis kit from Stratagene. *Escherichia coli* JM109 or APM was used for preparing all NMR samples. The APM strain is a derivative of JM109 that has enhanced growth characteristic in D_2O media (*42*). Typically, ∼400 mL of minimal medium culture was induced with 1.0 mM IPTG at an OD_{600} of ∼0.6, and cells were harvested ∼20 h after induction. Protein purification involved breaking the cells by sonication in lysis buffer [25 mM Tris-HCl (pH 7.8), 20 mM EDTA, and 50 mM β-mercaptoethanol], followed by ultracentrifugation of the lysate (30K rpm for 20 min, Beckman Ti70 rotor). The cleared lysate was chromatographed on a 150 mL CM50 column (Pharmacia) equilibrated with buffer A [25 mM Tris-HCl (pH 7.8), 5 mM EDTA, and 10 mM β-mercaptoethanol]. The protein was eluted from the column with a 600 mL 0 to 1.0 M NaCl gradient in the same buffer. Pooled fractions were loaded on a 10 mL *S*-hexylglutathione affinity column (Sigma) equilibrated with buffer B [25 mM Tris-HCl (pH 7.8), 2.8 mM EDTA, and 10 mM β-mercaptoethanol]. Elution of the bound protein was achieved using 50 mM glycine (pH 10.0). The fractions were adjusted to pH 7.0 with 0.2 volume of 1 M Tris-HCl (pH 7.0) immediately after elution. The purified enzyme was concentrated and exchanged into NMR buffer [10 mM potassium phosphate (pH 7.0), 25 μM EDTA, 50 mM NaCl, 0.02% sodium azide, and 5% D_2O] by ultrafiltration (Amicon) and/or dialysis (Spectra/Por). The typical yield of purified hGSTA1-1 was approximately 16 mg from 400 mL of D_2O M9 culture. An extinction coefficient (ϵ_{280}) of 19 000 M^{-1} cm^{-1} was used for quantifying the purified protein. The purified protein exhibited a single band when analyzed by SDS−PAGE and a correct mass of 25.5 kDa when analyzed by MALDI-TOF mass spectrometry. The specific activities of hGSTA1-1 and the hGSTA1-1 C112S mutant were indistinguishable at 40 μmol min^{-1} mg^{-1} (22.5 °C and pH 7.0). This is consistent with previous results showing that AEDANS modification, "glutathiolation", and

cross-linking by bismaleimides at Cys112 have little effect on the enzyme activity of hGSTA1-1 (*31*, *43*). The hGSTA1-1 C112S mutant was constructed and used for some of the NMR experiments because of slow changes in the GSH-bound hGSTA1-1 spectra that were thought to be associated with modifications of the cysteine residue in the protein. These spectral changes were later found to be due to oxidation of GSH in the NMR sample.

All NMR samples were prepared from cultures grown in 99.8% D_2O M9 medium. Uniform ^{15}N labeling was used, except for amino acid-specific ^{15}N-labeled samples. Samples used for ^{13}C backbone assignments were also labeled with [U-$^{13}C_6$]glucose. When specifically ^{15}N- and/or ^{13}C-labeled amino acids were used for labeling, the amino acids were added to the culture ~1 h before induction (150 mg/L Ala, 100 mg/L Pro, 100 mg/L aliphatic amino acids, and 50 mg/L aromatic amino acids). Isotopes were purchased from either Cambridge Isotope Laboratories or Sigma-Aldrich. Typical NMR sample concentrations were 1.0−1.3 mM (monomer concentration). GSH or EASG-bound NMR samples contained 10 mM ligand in NMR buffer. GSH-bound NMR samples were deoxygenated under nitrogen overnight, and the NMR tube was flushed with nitrogen before being capped. Deoxygenation is necessary; otherwise, the GSH is slowly oxidized to dimers, causing continual changes in the NMR spectra due to the ability of the dimer to bind to hGSTA1-1. EASG was chemically synthesized, essentially as described by Ploemen from EA and GSH (*44*). Its purity was checked with thin-layer chromatography and with ninhydrin (*45*). A single diastereoisomer of EASG was synthesized via the hGSTP1-1-catalyzed reaction from EA and GSH (*46*). hGSTP1-1 was expressed and purified as described previously (*40*). The enzyme-catalyzed reaction was performed in 40 mM potassium phosphate buffer (pH 6.5) using 0.1 mM hGSTP1-1 and 4 mM GSH in a 9 mL reaction volume. An equal molar amount of EA in a 1:1 ethanol/water mixture (200 μL) was added 10 μL at a time to the reaction mixture, and the pH was titrated to 6.5 using saturated $NaHCO_3$ after each addition. The reaction was filtered with a centriprep or a centricon (Amicon) to remove the enzyme. The filtrate was then lyophilized and redissolved with 300 μL of water. Concentrated phosphoric acid was added until precipitate no longer formed. The precipitate was then spun down, and the pellet was washed with 100 μL of water prior to the addition of 250 μL of water. Sufficient 1 M NaOH was added to dissolve the pellet and then to adjust the pH of the solution to 7.0. The quality of the EASG diastereoisomer was checked with one-dimensional proton NMR, and the ratio of the two diastereoisomers was higher than 7:1 (*46*).

NMR Spectroscopy. NMR experiments were performed using a Bruker DRX 600 MHz spectrometer equipped with triple-resonance probes, triple-axis pulsed-field gradient coils, and deuterium decoupling. Unless otherwise noted, experiments were carried out at 302 K. The typical recycle delay time is 1.4 s; 1024 complex points were recorded for the directly detected dimension in all NMR experiments.

For all experiments related to backbone assignments, including HMQC, two-dimensional (2D) HNCO, HNCO, HN(CA)CO, HN(CO)CA, HNCA, HN(CO)CB, HNCB, and four-dimensional (4D) HNNH-NOESY, quadrature detection was achieved using the States−TPPI method. The number of complex points recorded for ^{15}N was 32 for all three-dimensional experiments, and 20 for both 4D experiment dimensions. The sweep width of ^{15}N was always 29.6 ppm. For the HNCO, HN(CA)CO, HN(CO)CA, HNCA, HN(CO)CB, HNCB, and 4D HNNH-NOESY experiments, there were 8, 32, 16, 16, 32, 32, and 2 scans, respectively. The number of complex points and the sweep width were 48 and 13.3 ppm for CO, 56 and 26 ppm for C_α, and 32 and 37 ppm for C_β, respectively. The mixing time for the 4D NOESY experiment was 140 ms. Additional details regarding the above experiments can be found in McCallum et al. (*39*). The identification of some of the amino acid spin system types was done using 2D HNCO experiments (*39*) with uniformly ^{15}N-labeled, specifically 1-^{13}C-labeled NMR samples. In the 2D HNCO experiment, the only amide resonances that can be detected follow the 1-^{13}C-labeled amino acid in the primary sequence. The following 1-^{13}C-labeled amino acids were used: Ala, Ile, Val, Leu, Phe, Pro, and Tyr.

TROSY-based pulse sequences were used to study the effects of temperature on the spectra as well as for experiments directed toward detecting chemical exchange (CPMG, $R_{1\rho} - R_1$) and for exploring fast dynamics ($^1H-^{15}N$ hnNOE). These 2D experiments have 150 or 160 complex points recorded in the ^{15}N dimension, and each experiment took ~2.5−9 h. For the relaxation-compensated CPMG-TROSY experiments (*47*), four 2D spectra were obtained; two τ_{CPMG} times of 0.77 and 10 ms, each of these at a relaxation delay time of either 0 or 40 ms. For data analysis, the change in relaxation rates between the two τ_{CPMG} values (ΔR) was calculated for each residue. Forty-eight scans were acquired for each 2D experiment. The $R_{1\rho} - R_1$ measurements (*48*) were acquired with 16 scans and a recycle delay time of 2.5 s. The measurements were taken at spin-lock off-resonance frequencies of 86.1, 95.9, and 106 ppm. The relaxation times were 0, 20, 20, 40, 80, 120, 120, and 160 ms with off-resonance carrier frequencies at 86.1 and 95.9 ppm and 0, 10, 10, 20, 40, 60, 60, and 80 ms with an off-resonance carrier frequency at 106 ppm. The spin-lock field strength used in the experiment is 1060.9 Hz (*49*). The hnNOE measurement experiments (*50*) have a recycle delay time of 1.9 s and an NOE transfer time of 3 s, and 48 scans were acquired for each experiment. The samples used for the experiments described above were aged for 10 days to prevent systematic errors from intensity changes in the amide peaks due to deuterium−proton exchange.

The C112S mutant of hGSTA1-1 was used instead of the wild-type protein for most of the chemical exchange studies and hnNOE measurements of the GSH-bound form. The HSQC spectrum of the mutant is similar to that of the wild-type protein, and the specific activities of the two proteins are essentially equivalent.

NMR Assignments and Chemical Shift Analysis. Spectra were processed with Felix2000 (Accelrys) on a Silicon Graphics O2 workstation. The backbone assignment software Monte (*38*) was used for incorporating chemical shift connectivity, proton−proton NOE, amino acid type, characteristic chemical shift, and X-ray crystal structure (PDB entry 1GUH) information into the assignments. A [1-^{13}C]-Ile and [^{15}N]Phe doubly labeled sample and a [1-^{13}C]Lys and [^{15}N]Ile doubly labeled sample were also used for 2D HNCO experiments to unambiguously assign Ile219 and

Phe220. The secondary structure of residues was determined from their backbone chemical shifts using the program TALOS (*51*).

Relaxation Data Analysis. NMR relaxation data analysis was performed using data-processing scripts from Palmer (*52*), NONLIN (*53*), and other in-house-written scripts. For relaxation measurements, all amide peaks that do not overlap significantly with other peaks and have reasonably strong intensities were used for data analysis. For the relaxation-compensated CPMG-TROSY and $R_{1\rho} - R_1$ relaxation data, the peak intensities were fitted to a monoexponential decay. Errors in the intensities were estimated from duplicate experiments, and errors in the fitted relaxation rates were determined by Monte Carlo methods (*54*). For the hnNOE measurement data, errors in peak intensities were estimated from the baseline noise level in the spectra.

In the relaxation-compensated CPMG-TROSY experiments, the measured rate of transverse relaxation is

$$R(\tau_{CPMG}) = R_2 + R_{ex}(\tau_{CPMG}) \quad (1)$$

where R_{ex} is sensitive to τ_{CPMG} if there is chemical exchange present on the CPMG time scale (1−10 ms).

In the $R_{1\rho} - R_1$ measurement experiments, based on two-site fast exchange theory, the measured relaxation rate is (*52*)

$$R_{eff} = R_{1\rho} - R_1 = (R_2 - R_1)\sin^2\theta + R_{ex}\sin^2\theta \quad (2)$$

$$R_{ex} = (\delta\omega)^2 p_A p_B \tau_{ex}/(1 + \tau_{ex}^2\omega_e^2) \quad (3)$$

where R_{eff} is the observed relaxation rate, $R_{1\rho}$ is the relaxation rate in the rotating frame, R_1 and R_2 are the ^{15}N spin−lattice and spin−spin relaxation rates, respectively. θ is the angle between the static magnetic field and the effective magnetic field during the spin lock, R_{ex} is the contribution of exchange to the relaxation rate, assuming a two-site model, p_A and p_B are the population fractions at the two exchanging sites, $\delta\omega$ is the difference in chemical shifts between the two sites, and τ_{ex} is a measure of the average lifetime for exchange and is related to the forward and reverse rate constants $\tau_{ex}^{-1} = k_1 + k_{-1}$. ω_e is the strength of the effective rotating-frame spin-lock field. $\omega_e = \omega_1/\sin\theta$, where ω_1 is the spin-lock field strength.

If we assume that $R_2 - R_1$ is constant for most of the residues, then the presence of chemical exchange on the 0.1−1 ms time scale will cause an amide group to have an R_{eff} larger than those of other residues with similar θ values. On the other hand, if an amide group has significant motion on the picosecond to nanosecond time scale, the value of $R_2 - R_1$ may be smaller than those of the other amides, resulting in a smaller R_{eff} compared with other residues with similar θ values. If the chemical exchange is faster than milliseconds to microseconds, $R_{eff}/\sin^2\theta$ will be independent of ω_e since $\tau_{ex}\omega_e$ is much smaller than 1.

Ligand Binding. The kinetics of binding of GSH to hGSTA1-1 were investigated using titration experiments in which the ligand is added to a NMR sample with a known protein concentration. Resonance peaks that are affected by the binding of the ligand were selected for analysis. The cross sections in the nitrogen dimension were summed to give one-dimensional peaks in the proton dimension. Via a fitting of these data with the two-site exchange model (*55*), an estimation of k_{on}, k_{off}, and K_A values for GSH binding can be obtained. This technique could not be used for EASG due to the slow exchange rates.

Glutathione analogues, GOH (γ-Glu-Ser-Gly, Biopeptide) and methylglutathione (GS-Me, Sigma-Aldrich), were used to probe the effect of modification of the thiol group on GSH-induced conformational changes of hGSTA1-1. Both compounds were present at a concentration of 10 mM in the NMR samples.

Enzyme Kinetics and Inhibition. GST activities are measured using 1-chloro-2,4-dinitrobenzene (CDNB) as a substrate (*56*). The K_m of GSH was measured by keeping the CDNB concentration at 1 mM, which is essentially the highest practical concentration because of solubility issues. The K_i of EASG was determined by varying the GSH concentration in the presence and absence of 0.15 μM EASG with the CDNB concentration fixed at 1 mM. The data were analyzed assuming a random sequential or ordered sequential kinetic model. The K_i for EA was measured by varying the CDNB concentration in the presence and absence of 3.0 μM EA with the GSH concentration fixed at 1 mM. All kinetic measurements were performed at approximately 22.5 °C.

RESULTS

Resonance Assignments. Of the 209 non-proline residues in hGSTA1-1, it was possible to observe 202, 174, and 174 resonance lines from main chain amides in a ^{15}N−^{1}H HSQC spectrum of unliganded hGSTA1-1, the GSH complex, and the EASG complex, respectively. Of these, a total of 152, 151, and 148 resonances could be reliably assigned in the respective samples. Most of the CO, C_α, and C_β chemical shifts are assigned for these amide peaks. In general, the unassigned amide signals did not give observable cross-peaks in triple-resonance experiments used for assignments. Weak, or absent, cross-peaks in these NMR spectra are due to two main factors. First, buried residues give weak or nonexistent proton signals because they retain their amide deuteron after biosynthesis in D_2O. Second, enhanced spin−spin relaxation from other exchange processes can lead to signal loss during the three-dimensional NMR experiments.

The assignments for the C-terminal part of hGSTA1-1 are illustrated in Figure 2. Chemical shift assignments were achieved for this region of the protein in both the GSH-bound and EASG-bound forms, suggesting a stable well-defined conformation. The horizontal bars in each panel of Figure 2 indicate inter-residue connectivities based on CO, C_α, and C_β chemical shifts. The bottom part of the diagram provides information about how well measured NOEs agree with those predicted from the EASG crystal structure. As expected for an α-helical configuration, there are extensive i to $i + 1$ and i to $i + 2$ connectivities in this region of the protein. For the GSH-bound form, the assignments show broken inter-residue connectivities solely because of the degeneracy of the amide peaks for Glu214 and Glu215. Although all of the expected inter-residue scalar and NOE connectivities are present for these two residues, it is impossible to tell which resonance peaks belong to which of the two residues.

The secondary structures of the residues in the protein were predicted from the main chain chemical shifts using TALOS. On the basis of this analysis (not shown), the C-terminal

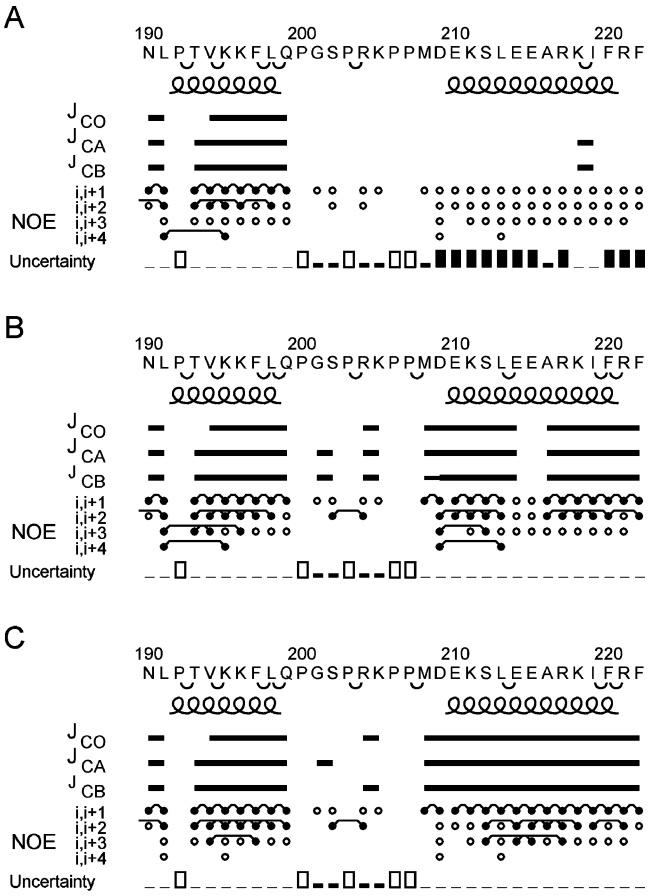

FIGURE 2: Backbone assignments of the C-terminal region of hGSTA1-1 in the unliganded (A), GSH-bound (B), and EASG-bound (C) forms. A section of the output from the assignment program Monte is shown. The primary sequence is given at the top of the diagram. The coils beneath the sequence represent α-helices. Half-circles connecting two adjacent residues below the sequence represent confirmed amino acid types by specifically 1-^{13}C-labeled samples. Solid lines show observed inter-residue connections for CO, C_α, and C_β chemical shifts. The section labeled NOE shows proton−proton NOEs predicted from the *S*-benzylglutathione-bound crystal structure [1GUH (*16*)]. Connections between filled circles represent observed NOEs, while empty circles represent interproton distances of less than 4.8 Å that were not detected in the 4D NOESY spectrum but exist in the crystal structure. The bottom line, labeled (Uncertainty), shows the degree of uncertainty for the assignments. Confident assignments are denoted by very short vertical bars, while unassigned residues have full-height filled bars. Proline residues are shown as empty bars.

region in both GSH and the EASG complex are predicted to be primarily in an α-helical conformation.

The unliganded form of the protein presents a completely different picture in terms of residue assignments for the C-terminus. Only a small number of confident assignments could be achieved; specifically, only Met208, Ala216, Lys218, and Ile219 could be assigned. Met208 and Ala216 were assigned on the basis of similar H_N, N, CO, C_α, and C_β chemical shifts as in the GSH and EASG-bound forms of the enzyme. The assignments of Lys218 and Ile219 were initially based on the same criteria but later confirmed by the observation of the expected cross-peak in the 2D HNCO spectrum of a sample labeled with [^{15}N]Ile and [^{13}C]Lys, as discussed above. It was not possible to analyze the secondary structure of the unliganded form using TALOS because of an insufficient number of assigned residues. However, the similarity of the chemical shifts to those in the GSH and EASG forms suggests that the secondary structures are similar.

It is not clear whether the remaining 11 residues in the C-terminal region give rise to observable amide resonances. Since there are no sharp peaks in the HMQC spectrum of unliganded hGSTA1-1, we can exclude the possibility that the remaining C-terminal residues undergo fast motion in a denatured state. Therefore, exchange broadening is the more likely explanation for our being unable to assign their amide resonances. We confirmed that there is no visible resonance peak for Phe220 in the unliganded enzyme by preparing a sample that was labeled with [^{15}N]Phe and [1-^{13}C]Ile and acquiring a 2D HNCO spectrum for an extended duration. The peak for Phe220 was absent in this spectrum, but readily appeared in this sample upon addition of GSH or EASG. In the case of the GSH-bound form, the resonance from Phe220 is weak, strongly suggesting the presence of chemical exchange. This was later confirmed in the CPMG-TROSY and $R_{1\rho} - R_1$ measurement experiments (see below). It was not feasible to determine the presence of resonances from additional C-terminal residues with double labeling schemes. Consequently, it may be possible that some C-terminal residues give observable, but weak and unassigned, peaks in the ^{15}N−^{1}H HSQC spectra.

During the course of these experiments, it became apparent that incubation of the enzyme with EASG over a period of several days leads to a modified form of the enzyme. This modification appears to occur at Cys112. The EASG-bound form of the wild-type enzyme shows two peaks with similar intensities for Glu115, Lys129, Phe220, and Phe222. A similar phenomenon is also seen in the [^{13}C]methyl resonances from two Met residues, one of which is Met208 and the other of which is likely Met105. These peaks are not caused by the presence of the two diastereoisomers present in the chemically synthesized EASG since the same effect was observed in the presence of a single diastereoisomer. The C112S mutant does not show double peaks for either the amide or methyl resonances. Consequently, we speculate that the thiol group of Cys112 acts as a weak nucleophile and displaces either the EA from EASG or one of the arylchlorides from the EA moiety of EASG. This ultimately leads to the covalent attachment of EA or EASG, respectively, to Cys112. This modification does not appear to change any of the functional properties of the enzyme, as the specific activities of both the wild-type and modified enzyme are identical. For the relaxation and chemical exchange studies, one of each of the double peaks from the four amide groups was chosen for analysis. However, both peaks appeared to give similar results.

Temperature Dependence of the HSQC Spectrum of Unliganded GSTA1-1. Temperature-dependent changes in peak shapes and intensities of NMR spectra provide useful information about the $\Delta H°$ of the transition between different conformational states. Using a sample labeled with [1-^{13}C]-Ile and [^{15}N]Phe, we were unable to observe a resonance for Phe220 in the unliganded sample over the temperature range of 277−307 K, suggesting that it remained in intermediate exchange throughout the entire temperature range.

The amide peak for Ile219 could be assigned in the spectra of unliganded hGSTA1-1. Temperature effects on this peak are shown in Figure 3. The amide peak of Ile219 becomes

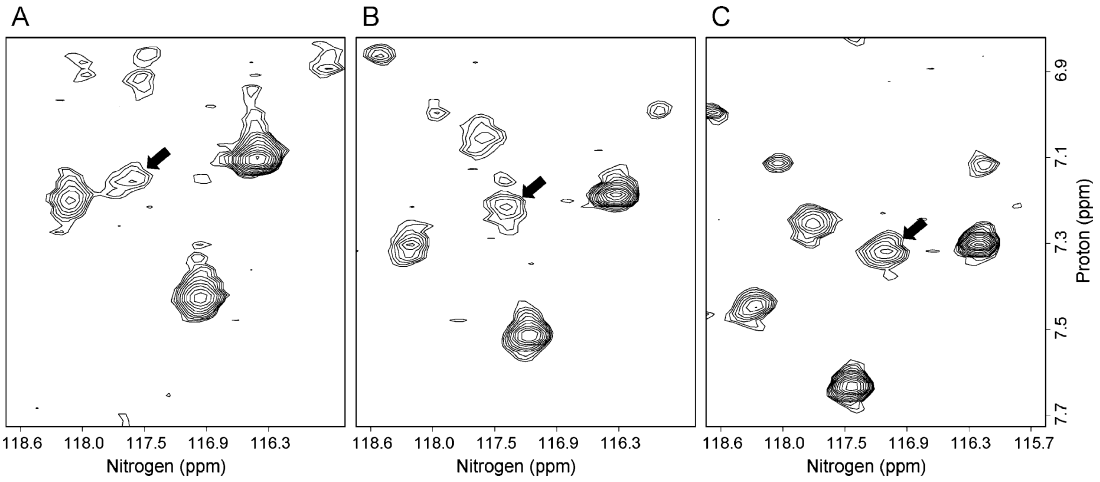

FIGURE 3: TROSY-HSQC spectra of unliganded hGSTA1-1 ([^{15}N]Ile specifically labeled) at 278 (A), 288 (B), and 302 K (C). The arrow points to the peak for the amide group of I219.

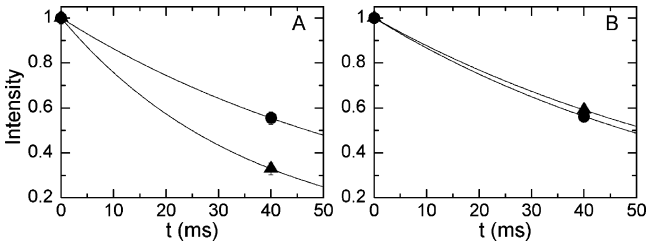

FIGURE 4: Amide nitrogen transverse relaxation measurements using relaxation-compensated CPMG-TROSY experiments for Ile219 in unliganded hGSTA1-1 (A) and the GSH-bound hGSTA1-1 C112S mutant (B). τ_{CPMG} values of 0.77 (●) and 10 ms (▲) are used.

significantly weaker at lower temperatures. This change in intensity is caused by chemical exchange between two or more conformations, proceeding from fast exchange at 302 K to intermediate exchange at 278 K. The fact that the Ile219 resonance does not sharpen at low temperatures, and that the resonance from Phe220 remains invisible over the entire temperature range, shows that the structural transition of the C-terminus is relatively unaffected by temperature. This is indicative of a small change in enthalpy as suggested by the stopped-flow studies of Atkins and co-workers (*28*).

Chemical Exchange with CPMG-TROSY Experiments. To characterize the exchange behavior of the C-terminal residues of hGSTA1-1, CPMG-TROSY transverse relaxation measurement experiments were performed on all three forms of the enzyme. If chemical exchange is occurring, the measured spin−spin relaxation rate (R) will become sensitive to the delay (τ_{CPMG}) between the refocusing pulses and different R rates will be obtained for different values of τ_{CPMG}. Chemical exchange will have the largest effect on R_2 if the average lifetime of the exchanging states is equal to τ_{CPMG}, i.e., on the time scale of 1−10 ms. Typical data that show the relaxation of the Ile219 resonance in unliganded and GSH-bound hGSTA1-1 are shown in Figure 4. For τ_{CPMG} times of 0.77 and 10 ms, the measured relaxation rates are 14.7 ± 1.7 and 27.8 ± 2.8 s^{-1} for unliganded hGSTA1-1, 14.4 ± 1.1 and 13.2 ± 1.0 s^{-1} for GSH-bound hGSTA1-1 C112S, and 13.3 ± 0.8 and 12.5 ± 0.8 s^{-1} for EASG-bound hGSTA1-1, respectively. A significant difference in the relaxation rates at the two different τ_{CPMG} values is observed in only the unliganded protein. Therefore, the amide group of Ile219 samples multiple environments in the unliganded

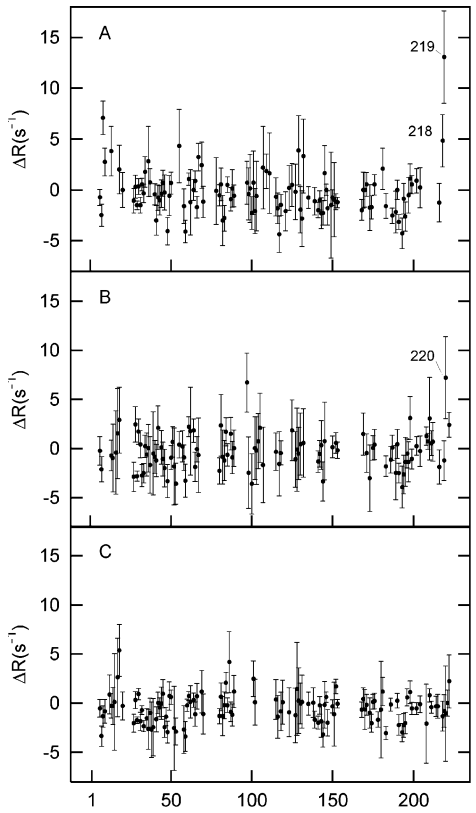

FIGURE 5: Backbone amide nitrogen transverse relaxation measurements of hGSTA1-1 in the unliganded (A), GSH-bound (C112S mutant) (B), and EASG-bound (C) forms. The differences in transverse relaxation rates (ΔR) at τ_{CPMG} times of 0.77 and 10 ms are plotted. Some residues are labeled on the plot to facilitate identification.

complex, but it does not undergo exchange in either the GSH or EASG complex.

The results for all residues that have been analyzed are summarized in Figure 5 as a difference in rates; $\Delta R = R(\tau_{CPMG}=10\text{ ms}) - R(\tau_{CPMG} = 0.77\text{ ms})$ for each residue. Overall, hGSTA1-1 does not show a significant amount of chemical exchange except for a small number of residues at both the amino and carboxy termini. In the unliganded protein, Ile219 and Lys218 are clearly affected by chemical exchange. The fact that two of the three C-terminal residues

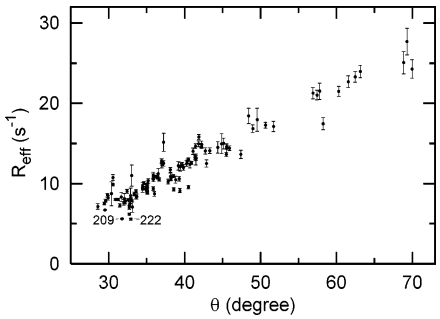

FIGURE 6: Results of amide nitrogen R_{eff} measurements for GSH-bound hGSTA1-1 with a spin-lock carrier offset of 19.6 ppm from the center of the ^{15}N spectrum. R_{eff} is the measured $R_{1\rho} - R_1$, and θ is the tilt angle between B_0 and the effective magnetic field during the spin lock.

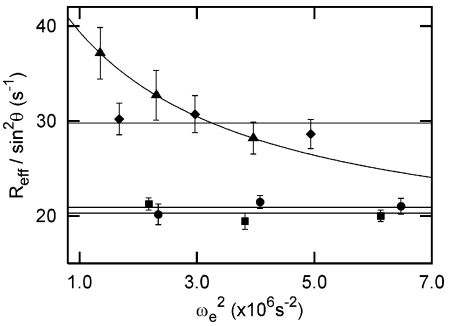

FIGURE 7: $R_{eff}/\sin^2\theta$ data plotted against ω_e^2 for Asp209 (●), Ile219 (◆), Phe220 (▲), and Phe222 (■) in the GSH-bound hGSTA1-1 C112S mutant. R_{eff} was measured at three different spin-lock offsets (9.5, 19.6, and 29.4 ppm from the center of the ^{15}N spectrum). Horizontal lines are plotted for residues Asp209, Ile219, and Phe222 along with the data points. A curve of the form $R_{eff}/\sin^2\theta = R_2 - R_1 + R_{ex}$, where $R_{ex} = (\delta\omega)^2 p_A p_B \tau_{ex}/(1 + \tau_{ex}^2\omega_e^2)$, is plotted along with the data points of Phe220. These curves are meant to guide the eye.

that could be analyzed exhibited signs of chemical exchange supports the contention that the unassigned resonances from this region of the protein are subject to exchange broadening.

In the GSH form, Phe220 exhibited the largest ΔR value of all of the residues, indicating that the amide group of this residue is experiencing multiple environments with different chemical shifts. In contrast to the situation in the unliganded enzyme, no significant chemical exchange was detected for Asp209, Glu210, Lys211, Ser212, Ala216, or Ile219. This indicates that these residues are not sampling different environments on the millisecond time scale. However, $R_{1\rho} - R_1$ and hnNOE measurements, which are discussed below, indicate that both Asp209 and Phe222 undergo motion on a time scale of nanoseconds to picoseconds. The C-terminal region of the EASG complex did not show any change in ΔR for residues 208, 210, 211, 214, 215, and 218−222, indicating that there is no chemical exchange on the millisecond time scale.

$R_{1\rho} - R_1$ Measurements of GSH-Bound hGSTA1-1 C112S. The fact that most of the C-terminal residues in the GSH-bound form did not show chemical exchange on the CPMG time scale was unexpected since GSH has limited contacts with the C-terminal helix (see Figures 1 and 8). Therefore, the motion of the C-terminal residues of the GSH-bound protein was investigated on a faster time scale using off-resonance spin-lock experiments. Figure 6 shows results for

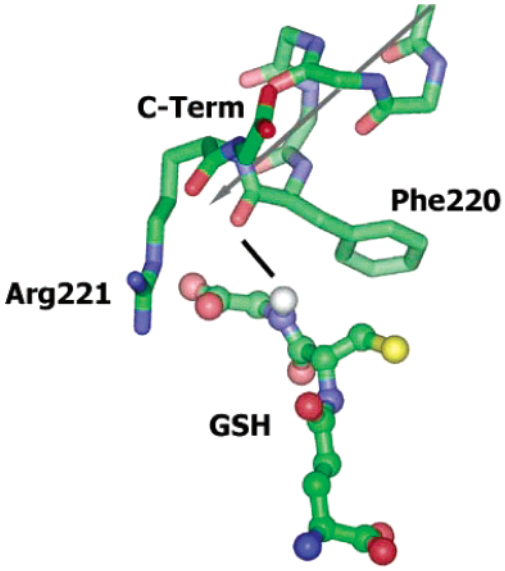

FIGURE 8: Interactions between bound GSH and C-terminal residues. The original coordinates were obtained from the EASG hGSTA1-1 complex (*15*), and the EA moiety was removed for clarity. The position of the side chain of Arg221 and the ϕ angle of the Gly residue in GSH have been altered as described in the text. The gray arrow shows the direction of the C-terminal α-helix. The putative hydrogen bond between H_N of GSH and the carbonyl oxygen of Phe220 is represented by a black line. Only the side chains of Phe220 and Arg221 are shown, interacting with C_β and the carboxyl group of the Gly residue within GSH, respectively. The side chain of Ile219 is not shown but projects into a hydrophobic pocket located behind the helix.

$R_{1\rho} - R_1$ measurements with the spin-lock field on 95.9 ppm. Data points for most of the residues are consistent with the relationship $R_{eff} = R_{1\rho} - R_1 = (R_2 - R_1)\sin^2\theta$, indicating that there is no chemical exchange on the time scale of 0.1−1 ms. Two C-terminal residues, Asp209 and Phe222, exhibited lower R_{eff} values that are indicative of shorter R_2 values due to motion on a time scale of nanoseconds to picoseconds.

To verify the presence or absence of chemical exchange, the dependence of $R_{eff}/\sin^2\theta$ on ω_e^2 was investigated for each residue, and this dependence is shown in Figure 7 for selected residues. It is clear that $R_{eff}/\sin^2\theta$ for Ile219, Asp209, and Phe222 is independent of the spin-lock field strength (ω_e), indicating a lack of exchange on the time scale of 0.1−1 ms. Similar results are obtained for other residues in the C-terminus (data not shown). The measured $R_{eff}/\sin^2\theta$ value of 30 s^{-1} is appropriate for the molecular mass of hGSTA1-1. In contrast, Phe220 shows signs of chemical exchange on the time scale of 0.1−1 ms because its $R_{eff}/\sin^2\theta$ value is affected by the strength of the spin-lock field.

In the cases of Asp209 and Phe222, their $R_2 - R_1$ values are approximately 20 s^{-1}. This decrease in relaxation rate is caused by motion on the sub-nanosecond time scale. Indeed, hnNOE measurements are consistent with this conclusion. While most residues exhibit an hnNOE of ∼0.85, Asp209 and Phe222 have NOE values of 0.18 ± 0.04 and 0.41 ± 0.06, respectively. The other two C-terminal residues that exhibit lower-than-normal hnNOE values are Phe220 and Lys211, with values of 0.66 ± 0.06 and 0.51 ± 0.05, respectively, suggesting that they also undergo motion on this time scale. A more detailed study of the high-frequency backbone dynamics of hGSTA1-1 is currently in progress.

Ligand Binding Kinetics and Populations of Intermediates. In GSH titrations, most resonance peaks that are affected by GSH binding exhibit intermediate exchange. The k_{on} and k_{off} values as estimated from titration data are on the order of 6×10^5 M^{-1} s^{-1} and 3×10^2 s^{-1}, respectively, giving an equilibrium binding constant of 2×10^3 M^{-1}. These rates roughly agree with previous results obtained from stopped-flow experiments (*29*). In contrast, EASG was found to be in slow exchange. Consequently, the off-rate was estimated to be less than 12 s^{-1} on the basis of the observation that amides that have ligand-induced chemical shift changes of approximately 120 Hz in proton showed very little line broadening from chemical exchange in a half-liganded sample. An off-rate that is slower than 12 s^{-1} is consistent with either of the k_{-1} and k_{-2} values determined by Nieslanik et al. (*28*); therefore, it is not possible to determine which kinetic step is responsible for the EASG-induced chemical shift changes.

Studies by Nieslanik et al. indicated that the C-terminus in the EASG−hGSTA1-1 complex should exist in an equilibrium between a disordered form and an ordered form. The ratio of the populations was estimated from kinetic rate constants to be ∼1:9 at 20 °C, with the ordered form more favored (*28*). We did not observe any evidence of two populations in the NMR spectra of EASG-bound hGSTA1-1 at 29 °C. However, it may be difficult to detect two populations if the ratio is less than 1:9.

Effect of Glutathione Analogues. Both GOH (γ-Glu-Ser-Gly) and *S*-methylglutathione (GS-Me) were used to probe how modification of the thiol group on GSH affects conformational changes in hGSTA1-1. It was expected that protein chemical shifts would be similar for GSH and these two analogues. Surprisingly, the amide resonances of the C-terminal residues could no longer be located in the GOH or GS-Me complex, based on a comparison to the GSH spectrum. Since we have not yet obtained the assignments of the GOH and GS-Me forms, we cannot state whether these peaks are absent in the spectrum due to exchange broadening or due to large changes in chemical shift. Regardless, it is clear that the GOH- and GS-Me-bound forms of the protein are different from the GSH-bound form. This difference may be due to the fact that GSH, when bound to the enzyme, will be substantially ionized given that the pK_a of the thiol group is 6.7 (*29*).

Binding Constants of EA and EASG. The binding constants for EA and EASG were estimated from enzyme inhibition studies (*44*). The K_i for inhibition of hGSTA1-1 by EA was measured to be 1.1 μM, which agrees with a previously reported value (*36*). Determining the K_i for EASG from the inhibition data depends somewhat on the kinetic model. If an ordered sequential mechanism is assumed for the CDNB−GSH conjugation reaction, the K_i for EASG is 0.07 μM. If a random sequential mechanism (*57*) and a K_m of 1 mM for CDNB are assumed, then the K_i of EASG is 0.04 μM. Regardless of the kinetic model, the K_i values determined in this study are significantly lower than the K_D of 1.8 μM calculated from stopped-flow measurements (*28*).

DISCUSSION

Our results clearly demonstrate that a disorder-to-order transition of hGSTA1-1 occurs upon binding of EASG, consistent with the X-ray crystal structures. However, the results presented here contradict previous ideas regarding the structure of the GSH−enzyme complex. In the X-ray structure of glutathione sulfonate-bound rGSTA1-1, the C-terminal helix was found to be in a location different from its normal location in the EASG complex (*26*). Fluorescence studies on the W21F/F222W mutant of rGSTA1-1 showed little change in fluorescence when GSH was bound to the enzyme, which suggested that GSH was insufficient to order the C-terminus of this enzyme (*26*). However, the fact that the C-terminal residues can be readily assigned in the hGSTA1-1 enzyme indicates that this part of the protein forms a well-defined structure in the GSH-bound form. Furthermore, the pattern of amide−amide proton NOEs indicates that the C-terminal residues are α-helical in conformation. Finally, the main chain torsion angles that are predicted from the chemical shifts are consistent with a C-terminal α-helix in the GSH complex.

The stabilization of the C-terminal helix by GSH can occur either via direct GSH−protein interactions or by allosteric changes in the protein structure induced by GSH binding. The crystal structure of EASG-bound hGSTA1-1 strongly suggests the former. Figure 8 illustrates the interactions between the C-terminal residues and bound GSH that are either present in the EASG−hGSTA1-1 structure or can be generated by minor modifications of that structure. The side chain of Phe220 forms van der Waals contacts with C_β of the Cys residue in the GSH part of the conjugate. The involvement of Phe220 in the binding of GSH is supported by kinetic measurements; alteration of Phe220 to Ala increases the off-rate of GSH by a factor of 2.8 (*29*). Additional interactions between the C-terminal helix and GSH can be generated by minor modifications of the structure. A change in the ϕ angle of the Gly residue in GSH by 10° will permit the formation of a weak hydrogen bond between the carboxyl group of Phe220 and the amide group of the Gly residue of GSH. In addition, an electrostatic interaction between the positively charged side chain of Arg221 and the negatively charged carboxyl terminus of GSH can be established by simply selecting another low-energy rotomer of the side chain of Arg221. Additional stabilization of the GSH-induced α-helical structure is provided by the side chain of Ile219; it becomes buried in a hydrophobic pocket provided by the side chain atoms of Phe220 and G-site residues Leu41 and Ala38. The fact that the amide group of Ile219 does not exhibit chemical exchange over a wide range of time scales indicates that this residue forms extensive interactions in the GSH complex that prevent its movement. Given these possible interactions, it is not surprising that the C-terminal α-helix of hGSTA1-1 is stabilized by GSH binding. Previous results obtained from the hGSTA1-1 I219A mutant show that the mutation makes the C-terminal region less stable in the absence of ligand; however, when GSH is present, the C-terminus appears to be as stable as in the wild-type enzyme (*58*). These results are consistent with I219 playing a role in stabilizing the C-terminal helix, but other interactions contribute significantly to stabilization of the region when GSH is bound.

Although an α-helical conformation is the predominant form of the C-terminus in the GSH complex of hGSTA1-1, it is also apparent from our relaxation studies that this region of the protein may be marginally stable. The relaxation

studies (hnNOE) and chemical exchange data show that residues at both ends of the helix undergo motion on the millisecond or picosecond time scale. Our preliminary studies with GSH analogues GOH and GS-Me indicate that the behavior of the C-terminal helix may be quite sensitive to what exactly occupies the G-site. Consequently, GSH analogues, such as glutathione sulfonate, may not be good models for the GSH-bound form in solution.

The low stability of the C-terminal helix may explain conflicting reports in the literature. The fluorescence experiments of Adman et al. (*26*) used an altered rGSTA1-1 (F222W) to investigate the effect of binding of GSH to rGSTA1-1. It is possible that the replacement of Phe222 with Trp destabilized the C-terminal helix in this isozyme. Alternatively, since Phe222 contacts only the ethacrynic acid part of EASG (see Figure 1), it is possible that the fluorescence of Trp222 is insensitive to GSH binding.

Information regarding the structure of the C-terminus in the unliganded form of the protein is limited by the lack of resonance lines from this region. However, it appears that its structure bears some resemblance to the α-helical conformation observed in the GSH or EASG complex. This conclusion is based on the absence of narrow peaks in the spectra of unliganded hGSTA1-1, showing that this region is not completely denatured. More compelling evidence comes from the similarity in the chemical shifts of the C-terminal residues in all three complexes. The dynamic properties of the C-terminus were investigated for the assigned residues, and chemical exchange on the time scale of 1−10 ms was detected in this region. The lack of a temperature-dependent change in the spectrum indicates that the enthalpy difference between these states is small. Overall, these results are best explained by a very flexible C-terminal α-helix that samples alternative conformations. This description agrees with the model described by Mannervik and coworkers that was based on the binding of GSH to hGSTA1-1 (*29*).

Our studies indicate that the class alpha enzyme shows trends in ligand-induced ordering similar to those we have previously characterized with the class pi enzyme (*40*). This ligand-induced ordering can provide thermodynamic assistance for product release. In the case of hGSTA1-1, the free energy of binding of the EASG conjugate ($\Delta G^\circ = -40.8$ kJ/mol) indicates tight binding of the product to the enzyme. The free energy of EASG binding is close to the sum of the individual free energies for GSH binding ($\Delta G^\circ = -18.9$ kJ/mol) and for EA binding ($\Delta G^\circ = -34.5$ kJ/mol). Small changes in the interaction of the enzyme with the substrates versus the product can account for the difference of 12.6 kJ/mol. Clearly, the enzyme faces a considerable thermodynamic hurdle in the release of its product. This hurdle has been lowered somewhat by the fact that the C-terminal region will become flexible in the unliganded protein, providing a positive ΔS that will disfavor rebinding of the product. It is interesting to speculate why regions of both hGSTA1-1 and hGSTP1-1 become ordered in the presence of GSH, given that ordering of the ternary complex would also provide the same thermodynamic advantage for product release. The principal advantage may be to decrease the susceptibility of these regions to proteolytic attack. Given the high concentration of GSH in tissues (10 mM), most of the enzyme would exist in the folded form that is more resistant to proteolysis.

ACKNOWLEDGMENT

We thank Virgil Simplaceanu for maintenance of the NMR facility and T. K. Hitchens for the collection of preliminary data for assignment purposes and valuable advice during the course of this work. We also thank B. Mannervik for his generous gift of expression vectors.

REFERENCES

1. Armstrong, R. N. (1997) Structure, catalytic mechanism, and evolution of the glutathione transferases, *Chem. Res. Toxicol. 10*, 2−18.
2. Mannervik, B., Ålin, P., Guthenberg, C., Jensson, H., Tahir, M. K., Warholm, M., and Jörnvall, H. (1985) Identification of three classes of cytosolic glutathione transferase common to several mammalian species: correlation between structural data and enzymatic properties, *Proc. Natl. Acad. Sci. U.S.A. 82*, 7202−7206.
3. Meyer, D. J., Coles, B., Pemble, E. E., Gilmore, K. S., Fraser, G. M., and Ketterer, B. (1991) Theta, a new class of glutathione transferases purified from rat and man, *Biochem. J. 274*, 409−414.
4. Meyer, D. J., and Thomas, M. (1995) Characterization of rat spleen prostaglandin H D-isomerase as a sigma-class GSH transferase, *Biochem. J. 311*, 739−742.
5. Pemble, S. E., Wardle, A. F., and Taylor, J. B. (1996) Glutathione S-transferase class kappa: characterization by the cloning of rat mitochondrial GST and identification of a human homologue, *Biochem. J. 319*, 749−754.
6. Board, P. G., Baker, R. T., Chelvanayagam, G., and Jermiin, L. S. (1997) Zeta, a novel class of glutathione transferases in a range of species from plants to humans, *Biochem. J. 328*, 929−935.
7. Board, P. G., Coggan, M., Chelvanayagam, G., Easteal, S., Jermiin, L. S., Schulte, G. K., Danley, D. E., Hoth, L. R., Griffor, M. C., Kamath, A. V., Rosner, M. H., Chrunyk, B. A., Perregaux, D. E., Gabel, C. A., Geoghegan, K. F., and Pandit, J. (2000) Identification, characterization, and crystal structure of the omega class glutathione transferases, *J. Biol. Chem. 275*, 24798−24806.
8. Coles, B., and Ketterer, B. (1990) The role of glutathione and glutathione transferases in chemical carcinogenesis, *Crit. Rev. Biochem. Mol. Biol. 25*, 47−67.
9. Tew, K. D. (1994) Glutathione-associated enzymes in anticancer drug resistance, *Cancer Res. 54*, 4313−4320.
10. O'Brien, M., Kruh, G. D., and Tew, K. D. (2000) The influence of coordinate overexpression of glutathione phase II detoxification gene products on drug resistance, *J. Pharmacol. Exp. Ther. 294*, 480−487.
11. Litwak, G., Ketterer, B., and Arias, I. M. (1971) Ligandin: a hepatic protein which binds steroids, bilirubin, carcinogens and a number of exogenous organic anions, *Nature 234*, 466.
12. Wang, T., Arifoglu, P., Ronai, Z., and Tew, K. D. (2001) Glutathione S-transferase P1-1 (GSTP1-1) inhibits c-Jun N-terminal kinase (JNK1) signaling through interaction with the C terminus, *J. Biol. Chem. 276*, 20999−21003.
13. Yin, Z., Ivanov, V. N., Habelhah, H., Tew, K., and Ronai, Z. (2000) Glutathione S-transferase p elicits protection against H_2O_2-induced cell death via coordinated regulation of stress kinases, *Cancer Res. 60*, 4053−4057.
14. Bruns, C. M., Hubatsch, I., Ridderstrom, M., Mannervik, B., and Tainer, J. A. (1999) Human glutathione transferase A4-4 crystal structures and mutagenesis reveal the basis of high catalytic efficiency with toxic lipid peroxidation products, *J. Mol. Biol. 288*, 427−439.
15. Cameron, A. D., Sinning, I., L'Hermite, G., Olin, B., Board, P. G., Mannervik, B., and Jones, T. A. (1995) Structural analysis of human alpha-class glutathione transferase A1-1 in the apo-form and in complexes with ethacrynic acid and its glutathione conjugate, *Structure 15*, 717−727.
16. Sinning, I., Kleywegt, G. J., Cowan, S. W., Reinemer, P., Dirr, H. W., Huber, R., Gilliland, G. L., Armstrong, R. N., Ji, X., Board, P. G., Olin, B., Mannervik, B., and Jones, T. A. (1993) Structure determination and refinement of human alpha class glutathione transferase A1-1, and a comparison with the mu and pi class enzymes, *J. Mol. Biol. 232*, 192−212.
17. Patskovska, L. N., Fedorov, A. A., Patskovsky, Y. V., Almo, S. C., and Listowsky, I. (1998) Expression, crystallization and

preliminary X-ray analysis of ligand-free human glutathione S-transferase M2-2, *Acta Crystallogr. D54*, 458−460.
18. Raghunathan, S., Chandross, R. J., Kretsinger, R. H., Allison, T. J., Penington, C. J., and Rule, G. S. (1994) Crystal structure of human class mu glutathione transferase GSTM2-2. Effects of lattice packing on conformational heterogeneity, *J. Mol. Biol. 238*, 815−832.
19. Ji, X., Zhang, P., Armstrong, R. N., and Gilliland, G. L. (1992) The three-dimensional structure of a glutathione S-transferase from the mu gene class. Structural analysis of the binary complex of isoenzyme 3-3 and glutathione at 2.2-Å resolution, *Biochemistry 31*, 10169−10184.
20. Ji, X., Armstrong, R. N., and Gilliland, G. L. (1993) Snapshots along the reaction coordinate of an SNAr reaction catalyzed by glutathione transferase, *Biochemistry 32*, 12949−12954.
21. Oakley, A. J., Lo Bello, M., Ricci, G., Federici, G., and Parker, M. W. (1998) Evidence for an induced-fit mechanism operating in pi class glutathione transferases, *Biochemistry 37*, 9912−9917.
22. Prade, L., Huber, R., Manoharan, T. H., Fahl, W. E., and Reuter, W. (1997) Structures of class pi glutathione S-transferase from human placenta in complex with substrate, transition-state analogue and inhibitor, *Structure 5*, 1287−1295.
23. Reinemer, P., Dirr, H. W., Ladenstein, R., Huber, R., Lo Bello, M., Federici, G., and Parker, M. W. (1992) Three-dimensional structure of class pi glutathione S-transferase from human placenta in complex with S-hexylglutathione at 2.8 Å resolution, *J. Mol. Biol. 227*, 214−226.
24. Rossjohn, J., McKinstry, W. J., Oakley, A. J., Verger, D., Flanagan, J., Chelvanayagam, G., Tan, K. L., Board, P. G., and Parker, M. W. (1998) Human theta class glutathione transferase: the crystal structure reveals a sulfate-binding pocket within a buried active site, *Structure 6*, 309−322.
25. Le Trong, I., Stenkamp, R. E., Ibarra, C., Atkins, W. M., and Adman, E. T. (2002) 1.3-Å resolution structure of human glutathione S-transferase with S-hexyl glutathione bound reveals possible extended ligandin binding site, *Proteins: Struct., Funct., Genet. 48*, 618−627.
26. Adman, E. T., Le Trong, I., Stenkamp, R. E., Nieslanik, B. S., Dietze, E. C., Tai, G., Ibarra, C., and Atkins, W. M. (2001) Localization of the C-terminus of rat glutathione S-transferase A1-1: crystal structure of mutants W21F and W21F/F220Y, *Proteins: Struct., Funct., Genet. 42*, 192−200.
27. Nieslanik, B. S., Dabrowski, M. J., Lyon, R. P., and Atkins, W. M. (1999) Stopped-flow kinetic analysis of the ligand-induced coil-helix transition in glutathione S-transferase A1-1: evidence for a persistent denatured state, *Biochemistry 38*, 6971−6980.
28. Nieslanik, B. S., Ibarra, C., and Atkins, W. M. (2001) The C-terminus of glutathione S-transferase A1-1 is required for entropically-driven ligand binding, *Biochemistry 40*, 3536−3543.
29. Gustafsson, A., Etahadieh, M., Jemth, P., and Mannervik, B. (1999) The C-terminal region of human glutathione transferase A1-1 affects the rate of glutathione binding and the ionization of the active-site Tyr9, *Biochemistry 38*, 16268−16275.
30. Dirr, H. W., and Wallace, L. A. (1999) Role of the C-terminal helix 9 in the stability and ligandin function of class α glutathione transferase A1-1, *Biochemistry 38*, 15631−15640.
31. Wallace, L. A., Sluis-Cremer, N., and Dirr, H. W. (1998) Equilibrium and kinetic unfolding properties of dimeric human glutathione transferase A1-1, *Biochemistry 37*, 5320−5328.
32. Wallace, L. A., and Dirr, H. W. (1999) Folding and assembly of dimeric human glutathione transferase A1-1, *Biochemistry 38*, 16686−16694.
33. Allardyce, C. S., McDonagh, P. D., Lian, L.-Y., Wolf, C. R., and Roberts C. K. (1999) The role of tyrosine-9 and the C-terminal helix in the catalytic mechanism of alpha-class glutathione S-transferase, *Biochem. J. 343*, 525−531.
34. Johnson, W. W., Liu, S., Ji, X., Gilliland, G. L., and Armstrong, R. N. (1993) Tyrosine 115 participates both in chemical and physical steps of the catalytic mechanism of a glutathione S-transferase, *J. Biol. Chem. 268*, 11508−11511.
35. Condreanu, S. G., Ladner, J. E., Xiao, G., Stourman, N. V., Hachey, D. L., Gilliland, G. L., and Armstrong, R. N. (2002) Local protein dynamics and catalysis: detection of segmental motion associated with rate-limiting product release by a glutathione transferase, *Biochemistry 41*, 15161−15172.
36. Lian, L.-Y. (1998) NMR structural studies of glutathione S-transferase, *Cell. Mol. Life Sci. 54*, 359−362.
37. Lian, L. Y., Allardyce, C. S., Moody, P. C. E., and Roberts, G. C. K. (2001) Structure and folding of glutathione S-transferase A1-1: structural transition and ligand interactions, *Chem.-Biol. Interact. 133*, 13−16.
38. Hitchens, T. K., Lukin, J. A., Zhan, Y., McCallum, S. A., and Rule, G. S. (2003) MONTE: An automated Monte Carlo based approach to nuclear magnetic resonance assignment of proteins, *J. Biomol. NMR 25*, 1−9.
39. McCallum, S. A., Hitchens, T. K., and Rule, G. S. (1999) Solution structure of the carboxyl terminus of a human class mu glutathione S-transferase: NMR assignment strategies in large proteins, *J. Mol. Biol. 285*, 2119−2132.
40. Hitchens, T. K., Mannervik, B., and Rule, G. S. (2001) Disorder-to-order transition of the active site of human class pi glutathione transferase, GST P1-1, *Biochemistry 40*, 11660−11669.
41. Stenberg, G., Bjornestedt, R., and Mannervik, B. (1992) Heterologous expression of recombinant human glutathione transferase A1-1 from a hepatoma cell line, *Protein Expression Purif. 3*, 80−84.
42. Balibar, C., Brandon, N., and Rule, G. S. (2004) A variant of *E. coli* strain JM109 with enhanced growth properties in perdeuterated minimal media (manuscript to be published).
43. Lyon, R. P., and Atkins, W. M. (2002) Kinetic characterization of native and cysteine 112-modified glutathione S-transferase A1-1: reassessment of nonsubstrate ligand binding, *Biochemistry 41*, 10920−10927.
44. Ploemen, J. H. T. M., van Ommen, B., and van Bladeren, P. J. (1990) Inhibition of rat and human glutathione S-transferase isoenzymes by ethacrynic acid and its glutathione conjugate, *Biochem. Pharmacol. 40*, 1631−1635.
45. Moore, S. (1968) Amino acid analysis: aqueous dimethyl sulfoxide as solvent for the ninhydrin reaction, *J. Biol. Chem. 243*, 6281−6283.
46. van Iersel, M. L. P. S., van Lipzig, M. M. H., Rietjens, I. M. C. M., Vervoort, J., and van Bladeren, P. J. (1998) GSTP1-1 stereospecifically catalyzes glutathione conjugation of ethacrynic acid, *FEBS Lett. 441*, 153−157.
47. Loria, J. P., Rance, M., and Palmer, A. G. (1999) A relaxation-compensated Carr-Purcell-Meiboom-Gill sequence for characterizing chemical exchange by NMR spectroscopy, *J. Am. Chem. Soc. 121*, 2331−2332.
48. Kempf, J. G., Jung, J., Sampson, N. S., and Loria, J. P. (2003) Off-resonance TROSY (R1 ρ − R_1) for quantitation of fast exchange processes in large proteins, *J. Am. Chem. Soc. 125*, 12064−12065.
49. Palmer, A. G., Kroenke, C. D., and Loria, J. P. (2001) Nuclear magnetic resonance methods for quantifying microsecond-to-millisecond motions in biological macromolecules, *Methods Enzymol. 339*, 204−238.
50. Zhu, G., Xia, Y., Nicholson, L. K., and Sze, K. H. (2000) Protein dynamics measurements by TROSY-based NMR experiments, *J. Magn. Reson. 143*, 423−426.
51. Cornilescu, G., Delaglio, F., and Bax, A. (1999) Protein backbone angle restraints from searching a database for chemical shift and sequence homology, *J. Biomol. NMR 13*, 289−302.
52. Akke, M., and Palmer, A. G. (1996) Monitoring macromolecular motions on microsecond to millisecond time scales by $R_{1\rho}$-R_1 constant relaxation time NMR spectroscopy, *J. Am. Chem. Soc. 118*, 911−912.
53. Johnson, M. L., and Frasier, S. G. (1985) Nonlinear least-squares analysis, *Methods Enzymol. 117*, 301−342.
54. Bevington, P. R., and Robinson, D. K. (1992) *Data Reduction and Error Analysis for the Physical Sciences*, 2nd ed. McGraw-Hill: New York.
55. Carrignton, A., and McLachlan, A. D. (1983) *Introduction to Magnetic Resonance With Applications to Chemistry and Chemical Physics* Harper & Row: New York.
56. Habig, W. H., and Jakoby, W. B. (1981) Assays for differentiation of glutathione S-transferases, *Methods Enzymol. 77*, 398−405.
57. Mannervik, B., and Askelof, P. (1975) Absence of a ping-pong pathway in the kinetic mechanism of glutathione S-transferase A from rat liver. Evidence based on quantitative comparison of the asymptotic properties of experimental data and alternative rat equations, *FEBS Lett. 56*, 218−221.
58. Mosebi, S., Sayed, Y., Burke, J., and Dirr, H. W. (2003) Residue 219 impacts on the dynamics of the C-terminal region in glutathione transferase A1-1: implications for stability and catalytic and ligandin functions, *Biochemistry 42*, 15326−15332.

BI0363329